DOI: 10.23784/HN116-03

Fusing ROV-based photogrammetric underwater imagery with multibeam soundings for reconstructing wrecks in turbid waters

An article by ROBIN ROFALLSKI, PATRICK WESTFELD, JEAN-GUY NISTAD, ANNETT BÜTTNER and THOMAS LUHMANN

Observation and monitoring of wrecks are an integral part of the duties of hydrographic offices such as BSH. A common practice consists of first surveying wrecks using vessel-based multibeam echo sounding systems and subsequently having divers visually inspect them. In order to provide an objective procedure and set a baseline for monitoring wrecks, unmanned underwater vehicles equipped with imaging systems can be used to inspect wrecks and other obstructions in more details. This paper presents a workflow for combining multibeam soundings and photogrammetric point clouds generated by a ROV-based camera system. Structure from motion and image enhancement are used to obtain a colour-coded point cloud, which is then fused and scaled with the multibeam soundings, resulting in data densification on wrecks. Finally, the feasibility of integrating this fused data to common hydrographic practice is demonstrated.

ROV | underwater photogrammetry | multibeam echo sounder | point cloud fusion
ROV | Unter-Wasser-Photogrammetrie | Fächerecholot | Punktwolkenfusion

Wracks zu suchen und zu überwachen gehört zu den Aufgaben von Hydrographischen Diensten wie dem BSH. In der Praxis ist es gängig, Wracks zunächst mit schiffsgestützten Fächerecholotsystemen zu vermessen und anschließend von Tauchern visuell inspizieren zu lassen. Um ein objektives Verfahren bereitzustellen und eine Ausgangsbasis für die Überwachung von Wracks zu schaffen, können unbemannte, mit bildgebenden Systemen ausgerüstete Unter-Wasser-Fahrzeuge eingesetzt werden, mit denen Wracks und andere Hindernisse genauer inspiziert werden. Dieser Beitrag stellt einen Arbeitsablauf zur Kombination von Fächerecholotpeilungen und photogrammetrischen Punktwolken vor, die von einem ROV-basierten Kamerasystem erzeugt werden. Strukturen aus Bewegung und Bildverbesserung werden verwendet, um eine farbcodierte Punktwolke zu erhalten, die dann mit den Fächerecholotpeilungen verschmolzen und skaliert wird, was zu einer Datenverdichtung bei Wracks führt. Schließlich wird gezeigt, dass die Integration dieser verschmolzenen Daten in der hydrographischen Praxis machbar ist.

1 Motivation and state of the art

Mapping underwater obstructions (e.g. wrecks, rock fields) is a crucial mandate for the German Federal Maritime and Hydrographic Agency (Bundesamt für Seeschifffahrt und Hydrographie, BSH) and other institutions involved in safety of navigation around the world. BSH alone is responsible for monitoring more than 2,500 underwater obstructions in German territorial waters, regarded as potential hazards to shipping and fisheries (BSH 2020).

BSH presently carries out surveys of wrecks in a two-stage process. Hydrographic vessels first survey the wrecks using multibeam echo sounding systems (MBES) to obtain a georeferenced 3D point cloud, i.e. sounding set. This data set provides essential preliminary information (e.g. position, shape, height above seafloor) to professional divers, who subsequently inspect the wrecks with the aim of providing an accurate portrayal of their state. This process involves a detailed visual and tactile inspection as well as an independent measurement of the wrecks' shoalest point using a pneumatic depth sensing hose pipe. Remotely operated vehicles (ROV) equipped with camera systems sometimes supplement or partially replace the work of divers. Any potential change (e.g. collapse, sedimentation, drift) from the previous known state of a wreck is subsequently reported.

Vessel-mounted MBES are widely established for collecting bathymetry and detecting objects underwater (Brisette et al. 1997). Wide swaths and numerous narrow beams allow for efficient object detection and identification, even in turbid envi-

Authors
Robin Rofallski is a research assistant at Jade University in Oldenburg.
Dr. Patrick Westfeld, Jean-Guy Nistad and Annett Büttner are employed at BSH in Rostock.
Prof. Dr. Thomas Luhmann teaches at Jade University in Oldenburg.

robin.rofallski@jade-hs.de

ronments. Moreover, sounding measurement uncertainties not exceeding the IHO specification for Special Order Surveys (IHO 2008) provide a geometrically realistic representation of these objects. Unfortunately, the range and depression angle between the MBES and the object inevitably affect the sounding measurement accuracy and, more importantly in this use case, the ability to ensonify all parts of the object, especially on complex objects such as wrecks. A reliable assessment of the state of wrecks solely based on sounding measurements is therefore questionable. Professional divers and camera-equipped ROV provide the necessary close range in-situ inspection. However, due to poor visibility conditions, this inspection is much localised. A thorough assessment of the state of large objects (e.g. wrecks) is necessarily the synthesis of many such localised inspections, which is inherently subjective and error-prone.

Series of close-range underwater images collected by a camera-equipped ROV over wrecks, whilst still localised, are much easier to amalgamate to portray the whole structure of a wreck. Cameras are portable and small, thus being easily mountable on ROVs or attached to divers. Data in occluded areas is collected by simply circling the object. Photogrammetric analysis carried out on these images results in geometrically-correct three-dimensional point clouds characterised by high spatial and temporal resolution as well as colour information (Luhmann et al. 2020). When the imagery-based 3D point cloud is co-registered to the MBES soundings, the result is a fused data set characterised by higher data density and additional attribution (i.e. colour information). Moreover, targeting the ROV-images to the areas with low sounding densities (i.e. occluded areas) allows for an improved assessment of the state of a wreck. Finally, being fixed to a common terrestrial reference system, the fused data set is easily transferrable to the spatial data infrastructure of maritime administrations.

Fusing MBES data with information generated from cameras is thus highly desirable. However, underwater imagery suffers from many degrading and altering effects. This includes multimedia effects, as light travels through air, glass and water and thus, according to Snell's law, the ray is refracted twice at the interfaces. This, by definition renders the pinhole model invalid if no constructional corrections are employed. Strict modelling of the ray path has been developed, e.g. by Kotowski (1988), Maas (1995) and Jordt-Sedlazeck and Koch (2012). Several authors on the other hand found that when the camera is positioned close to a flat glass interface and oriented perpendicularly to it, refraction effects can be compensated by standard lens correction functions, as in Brown (1971), and strict modelling is only decisive in applications where highest accuracy is demanded (Kotowski 1988; Przybilla et al. 1990; Shortis 2015; Kahmen et al. 2019). Furthermore, the entrance pupil of a camera lens can be adjusted with the centre of a hemispherical dome port. This accounts for image degradation, and possible residual errors are compensated by standard lens correction functions (Menna et al. 2016). Furthermore, optical degradation from wavelength dependent light absorption, chromatic aberration or dispersion reduces image quality. This results in images with low contrast, colour cast, blur and haze (Wang et al. 2019). To account for these, several image enhancement and restoration algorithms have been developed over the years. These take the actual image formation model into account (e.g. Akkaynak and Treibitz 2019) or employ appropriate image processing tools, such as histogram stretching, white balance shift or gamma stretch to increase contrast, decrease colour cast, etc. In Bianco et al. (2015), the LAB method is introduced. Here, using a grey-world assumption, the chromatic component of the LAB colour space is shifted towards the white point and the luminance component is enhanced by histogram stretching and cut off. Thus, the method belongs to the latter kind of algorithms. Mangeruga et al. (2018) compared five state-of-the-art image enhancement algorithms for underwater photogrammetry and provided a metric for benchmarking these. It was concluded that for 3D reconstruction purposes, images enhanced with the LAB algorithm or the original images perform best on their data sets.

As photogrammetry cannot provide absolute positioning, further sensor data has to be combined with the imagery, providing a georeferenced position and point cloud. Furthermore, imagery can be used for online algorithms, solving positioning and mapping of the environment in real time (simultaneous localisation and mapping, SLAM). These algorithms suffer from drift, as they can only take a certain amount of data points and positions into account, in order to not overflow the memory and reduce computational complexity. Hence, the system drifts with time and distance travelled, thus requiring additional information for applications demanding high accuracy (Durrant-Whyte and Bailey 2006). Originating from the robotics community, SLAM is a broad research field and several methods have been proposed in recent years, using various kinds of sensors. State-of-the-art algorithms are proposed by Mur-Artal and Tardós (2017) or Engel et al. (2015), creating sparse or semi-dense point clouds respectively. These algorithms are capable, provided pre-calibrated cameras, of computing point clouds and provide localisation within the point clouds in real-time, depending on the image resolution. Furthermore, they automatically identify revisited areas and compute so-called loop-closures, i.e. creating consistency between non-sequential parts of the data

by bundle adjustment over all included observations.

Mapping underwater structures using photogrammetric techniques as the only acquisition method, or as part of a multi-sensor system, has been widely performed in tasks such as reef monitoring (Fabri et al. 2019), inspection of ship hulls (Kim and Eustice 2013) or cave surveying (Nocerino et al. 2018). Ship wrecks were observed and modelled by Prado et al. (2019) by fusion with MBES data. Further examples of photogrammetric wreck surveys, mostly in relatively clear water conditions, can be found in Drap et al. (2015) or Nornes et al. (2015).

2 Methodology

This paper presents data from a campaign carried out by BSH and Jade University of Applied Sciences, surveying a sunken former German air force vessel from WWII, 25 m in length and about 4 m in width. The wreck is located at a depth of about 14 m (relative to NHN) in the Bay of Neustadt (Baltic Sea). The MBES data was collected from the hydrographic survey vessel VWFS *Deneb*, operated by BSH. A ROV equipped with a camera to acquire imagery for photogrammetric analyses was subsequently deployed from the vessel. The resulting point cloud was fused with the MBES data in order to georeference the photogrammetric imagery.

2.1 Multibeam echo sounder data set

The MBES data set was collected from *Deneb* using a Teledyne-Reson Seabat 7125-SV2 (400 kHz) with 512 beams per swath. The software Teledyne PDS was used for real-time data acquisition and quality control. Five survey lines were collected over the wreck, three in the west-east direction and two in the north-south direction. The data was further post-processed using Teledyne-CARIS HIPS & SIPS. Fig. 1 shows the 0.10 m depth raster generated from the sounding data over and in the vicinity of the wreck. The wreck consists of about 71,866 points over an area of 203.5 m^2.

The total sounding uncertainty was calculated based on all estimated and measured uncertainty sources and propagated to the 3D position of the soundings. The soundings comprising the wreck have an uncertainty of 15 cm at the 95 % confidence level.

2.2 ROV and imagery data set

The ROV observations were carried out with a SAAB SeaEye Falcon ROV (Fig. 2, left). The ROV has a depth rating of 300 m and is capable of carrying up to 8.5 kg of additional payload. As the on-board ROV-camera did not provide sufficient resolution and stability for these photogrammetric analyses, an additional industrial-grade Basler Ace camera was mounted in a pressure housing on top of the

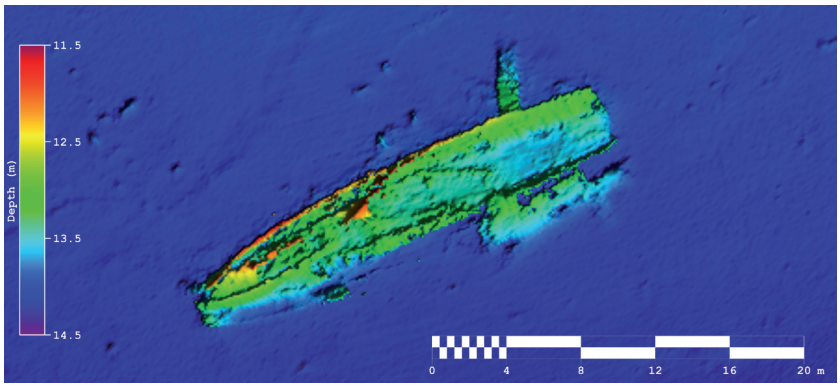

Fig. 1: Plan view of a 10 cm raster of the MBES sounding data set of the wreck. Colour coding depicts depth

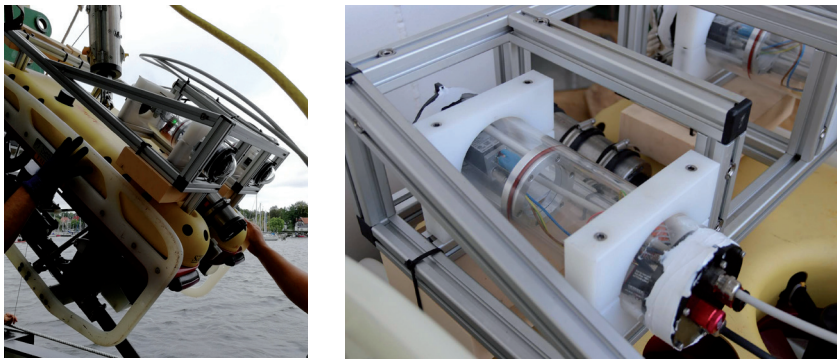

Fig. 2: ROV equipped with camera system on top (left) and camera in pressure housing (right)

ROV (Fig. 2, right). Relevant technical specifications are summarised in Table 1 and Table 2.

The camera housing was equipped with a hemispherical port to reduce image degradation introduced by the optical properties of water. These include mainly refraction and dispersion as a perfectly centred port would eliminate these effects completely and work as an additional lens element in the ray path. Deviations due to imperfect fitting of the dome can mostly be compen-

Saab SeaEye Falcon	
Maximum depth	300 m
Forward speed	> 3 kn
Weight	55 kg
Dimensions	1000 mm × 600 mm × 500 mm
Maximum added payload	8.5 kg

Table 1: ROV specifications

Basler Ace acA1920-48gc	
Sensor size	9.2 mm × 5.8 mm
Resolution	1920 px × 1200 px
Maximum frame rate	50 Hz
Pixel pitch	4.8 µm × 4.8 µm
Focal length	4.8 mm

Table 2: Camera specifications

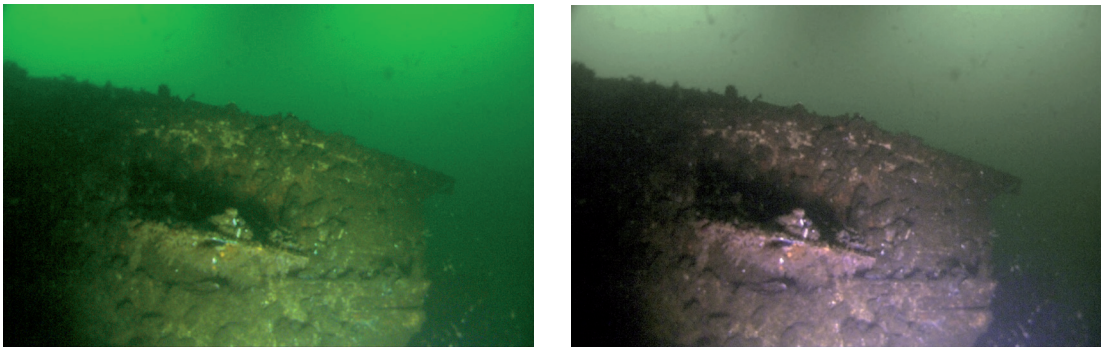

Fig. 3: Original image (left) and enhanced image using LAB algorithm (right)

sated by image distortion parameters (Menna et al. 2016; Nocerino et al. 2016). Otherwise, the ray path could be modelled explicitly by applying ray tracing approaches. This however, would require a specific bundle adjustment solution, eliminating the option of using standard structure-from-motion (SfM) software, as it is commercially available to users from administration and industry.

Images were acquired at a frame rate of 20 Hz. However, in order to reduce computational and memory effort, images were analysed at 2 Hz. At approximately 0.5 m/s lateral movement speed, an acquisition distance of 1 m and a ground sampling distance (GSD) of 1 mm has been achieved, this leads to an average overlap of 87 % in horizontal and 79 % in vertical direction. This is considered enough overlap to be able to robustly identify identical features over several images in a sequence. The total survey time, including dive time and time to locate the wreck, was about 15 min. of which 7.5 min. consisted in the imagery acquisition time.

The Baltic Sea has a high turbidity and therefore does not provide very good visibility conditions. In order to improve matching results and colour correctness, several image enhancement methods, as proposed in Mangeruga et al. (2018) were compared. By far the best results were achieved, using the LAB enhancement algorithm, proposed by Bianco et al. (2015). Fig. 3 displays a wreck feature viewed in the original image and the same feature viewed in an image enhanced by the LAB algorithm. The original image is obviously biased towards green, which distorts the wreck feature and reduces contrast. The enhanced image on the other hand still has a green background but the wreck feature is more distinguishable from the background. This leads to improved matching results.

Using the enhanced imagery, photogrammetric analyses were performed using structure-from-motion (SfM) processing methods. SfM techniques (e.g. Snavely et al. 2006; Furukawa and Ponce 2010) generate 3D representations from 2D image sequences without initial information. Feature points are extracted from the images and matched, employing robust estimation techniques such as RANSAC (random sample consensus; Fischler and Bolles 1981). Using these corresponding image points in multiple images, bundle adjustment was performed using a self-calibration approach. From this method, the interior orientation was calculated using distortion parameters according to Brown (1971), i.e. principal distance, principal point, radial-symmetric and decentering distortion, and affinity and shear. Simultaneously, values for exterior orientation (6DOF position of camera in object space) and 3D coordinates of the object points were estimated. The aforementioned steps were performed, using Agisoft Metashape, a widely used SfM software that has been proven to be robust in underwater photogrammetry (Mangeruga et al. 2018). Unfortunately, due to the commercial aspect of the software, no detailed insights are provided about the algorithms used for orientation and subsequent dense image matching (Remondino et al. 2013). For this image bundle, 606 images from the starboard side were aligned with

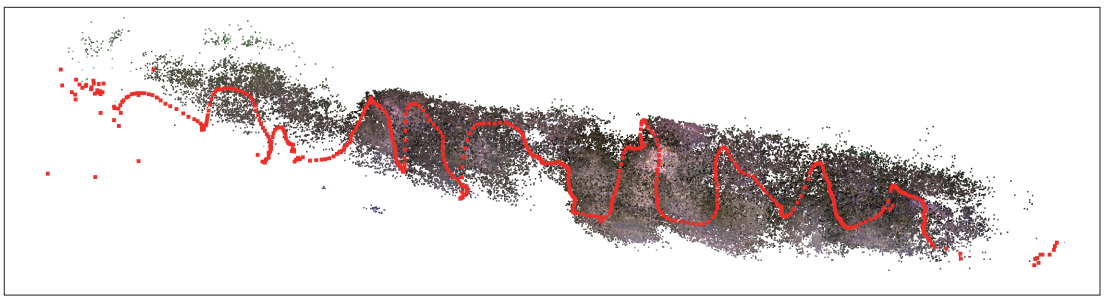

Fig. 4: RGB-coloured sparse point cloud and camera trajectory (red)

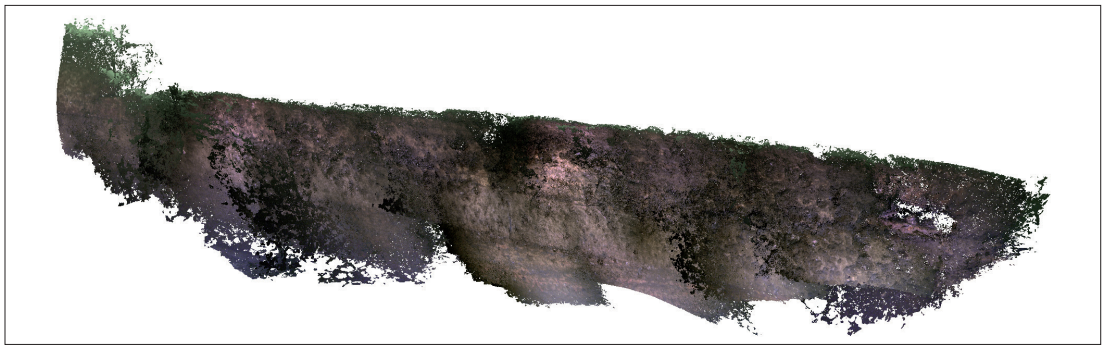

Fig. 5: Coloured dense point cloud of starboard side

132,516 tie points and used for all further processing steps (Fig. 4). Using unprocessed imagery, only 440 images were aligned with a significantly smaller covered area on the ship hull. Thus, for further processing, the enhanced imagery was used.

It is observable that the exterior orientations form a long stretched trajectory along the ship hull, starting on the right hand side. On the far left side, the distance to the object increases significantly, resulting in several images that could not be aligned due to turbid visibility and thus insufficient valid observed tie points in the images.

The RMS (root mean square) of the reprojection error was 1.50 px, equivalent to 1.5 mm in object space, assuming an average acquisition distance of 1 m. This rather low accuracy for photogrammetric applications probably originated from high turbidity and low contrast in the underwater imagery and a long stretched object that posed a dead-reckoning problem. However, this postulated accuracy only refers to the internal accuracy of the image bundle after adjustment. An exterior accuracy by comparing length measurement errors or cloud-to-cloud distances to a reference is not possible, as only a monocular system is used. Thus, neither an independent absolute scale can be provided nor was it possible to position a static reference object near the wreck with which to control results. However, if no significant deviations exist in a cloud-to-cloud comparison, it can be concluded that the photogrammetric point cloud achieves at least the same accuracy as the MBES data does, which is to be expected.

Using the aligned sparse point cloud, dense image matching was performed. According to the work of Remondino et al. (2013), a method similar to semi-global matching (Hirschmüller 2008) is used, though this has not been confirmed by Agisoft. Using the integrated algorithm, a dense point cloud consisting of 12.3 million points is created using »High« quality settings in the software. Processing, including the calculation of depth maps, took approximately four hours on an Intel Core i7 with 16 GB RAM. The resulting point cloud is shown in Fig. 5.

3 Data fusion

Fig. 6 shows the flow chart of the data fusion including all preprocessing steps before registration. Both photogrammetric and MBES data sets were adjusted individually in their respective coordinate systems and then combined by point cloud analysis methods. Absolute scaling was provided by the MBES data, thus providing absolute scale for photogrammetric data as well. In a practical solution and in order to control results, an independent scaling would be desirable by e.g. using a second camera for stereo analysis. Two independent point clouds can then be fused, deviations in scale evaluated, and possible errors identified.

Firstly, the two point clouds were coarsely aligned by selecting salient points. For that, the front tip of the wreck's bow and other salient points on the top of the wreck's starboard side were manually measured in the imagery and 3D coordinates determined. This process could be automatised by automatically identifying salient features in a resulting point cloud or applying a reference

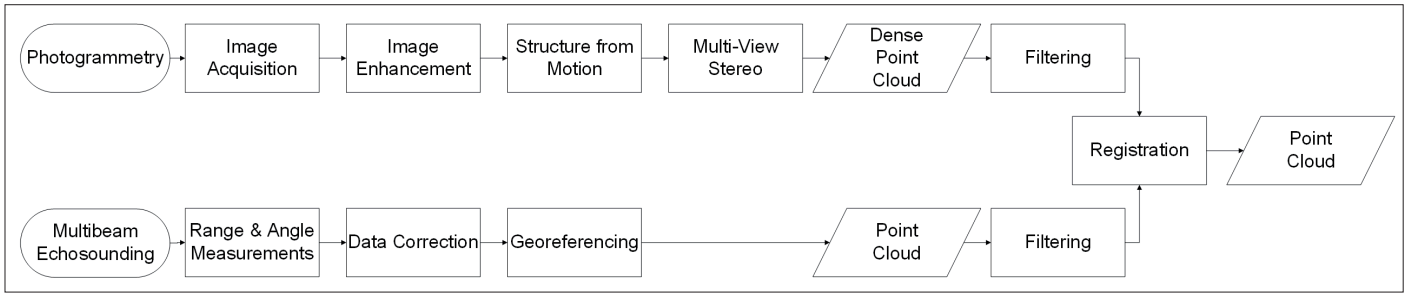

Fig. 6: Data processing and fusion to combine data from both photogrammetric analysis and MBES

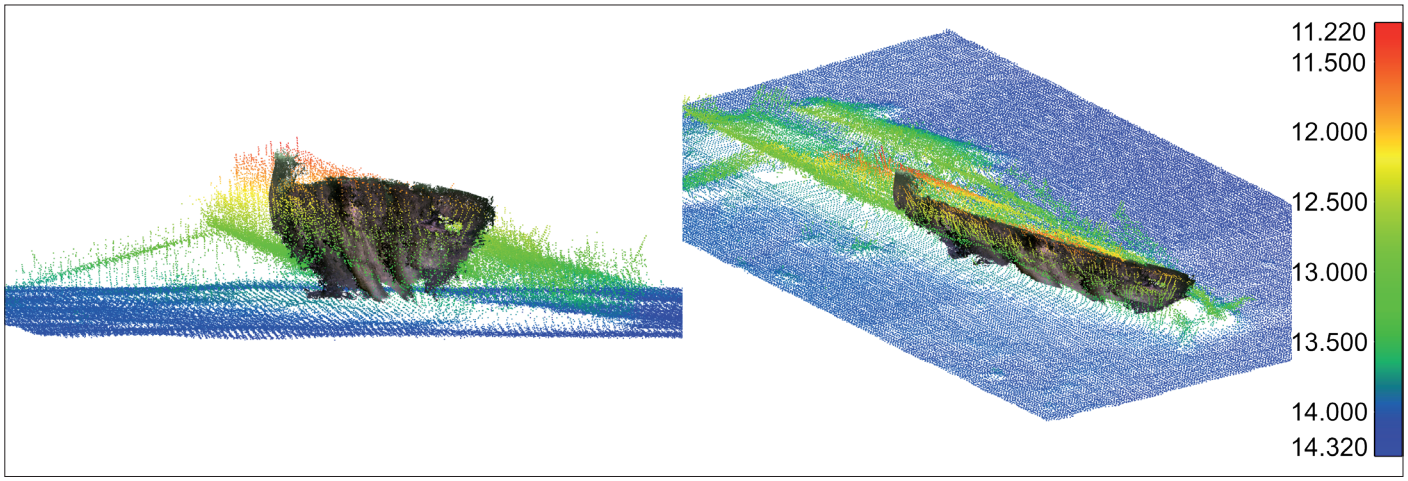

Fig. 7: Fused point clouds by photogrammetric analysis (RGB) and MBES soundings (coloured points) in side view (left) and isometric view (right). The dense point cloud filled areas lacking MBES soundings due to occlusion, such as on the bottom of the wreck. Colour scale depicts depth in metres

code to the ground control points. After coarse alignment, fine registration was performed using the Iterative Closest Point (ICP) algorithm (Besl and McKay 1992). The result is a georeferenced point cloud in ETRS89/UTM coordinates, which can be directly integrated in the following data processing chain of BSH hydrographic surveying. The hybrid origin of the data includes furthermore RGB colour values and MBES backscatter values that can be attributed to the points. Additionally, the photogrammetric imagery can be transformed to the relevant terrestrial reference system and stored, as well, providing a georeferenced image database for further information on the wreck.

3 Results

Fig. 7 shows an overlayed photogrammetric coloured point cloud with the MBES data. The data depicts the starboard side of the wreck's bow. The area covered by the photogrammetric point cloud is about 13 m × 2 m, which is approximately half of the wreck's length and almost the entire height above the seafloor on the starboard side.

It is clearly visible that the photogrammetric point cloud has a significantly higher point density and provides colour information. Furthermore, occluded areas near the bottom of the wreck can be observed with the photogrammetric data and thus provides completion of the data in these areas. This is observable in Fig. 7 (left), where areas of the wreck's bottom are filled with points in areas that were occluded to the MBES and thus not covered entirely. For accuracy evaluation, cloud-to-cloud distances were calculated, using least squares planes on the MBES data (Low 2004). Distances from the photogrammetric point cloud to local planes of the MBES data are calculated and shown in Fig. 8. The mean cloud-to-cloud distance is 0.053 m. Though not fully representative of the absolute accuracy achieved by this method, these numbers represent a measure of internal accuracy for the combination of both data sets. Apart from that, higher deviations occur in the lower part of the point cloud in areas that are not as densely covered as the rest of the point cloud.

Comparing point densities, the MBES point cloud was reduced for the subset with the closest points to the photogrammetric point cloud. The

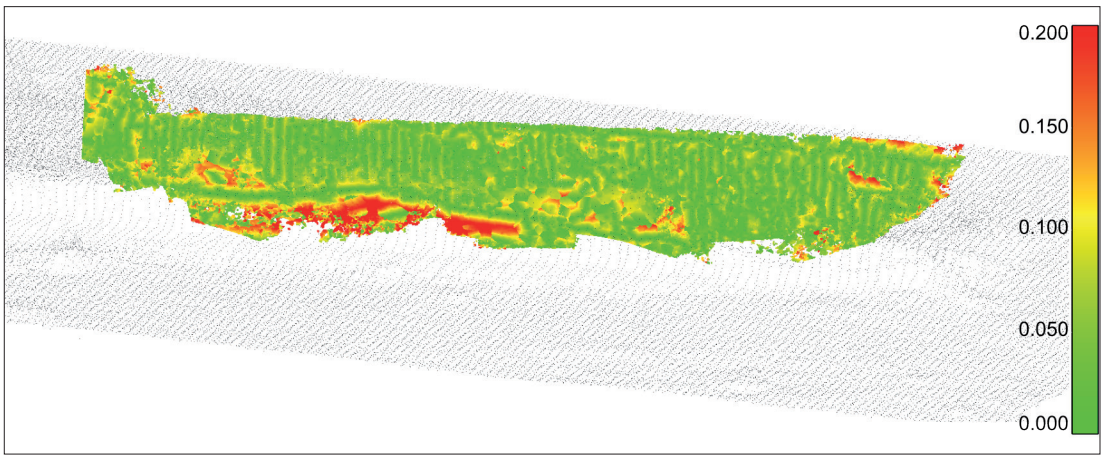

Fig. 8: Cloud-to-cloud distances referenced to least squares planes on MBES point cloud (scale unit in metres)

resulting reduced point cloud of MBES and the photogrammetric point cloud were then analysed for the surface density. This measure calculates the amount of points in a given neighbourhood to estimated planes of a radius R and extrapolates this number to 1 m². R was chosen to 20 cm, i.e. approximately 2 × GSD of the MBES data. As the investigated structure was mostly flat, this metric was chosen over the volumetric density. Table 3 shows the number of points and densities next to the total area covered by the given data set. It is worth mentioning that the covered area is estimated by projecting the point clouds to a plane and then calculating the area of the enclosing polygon. Thus, the amount of points cannot be simply divided by the covered area to obtain the mean surface density.

The table prominently shows the complementary characteristics of the two sensors. Where, on the one hand, the photogrammetric data had a high density with several hundred thousand points per square metre, the MBES provided a very much higher coverage of the area in a comparable amount of time needed for each of the methods.

Data set	Number of points	Area covered [m²]	Surface density [pts/m²]
MBES full	160,661	498	255
MBES closest points	3,791	22	158
Photogrammetry	12,324,258	22	535,069

Table 3: Point density metrics of the photogrammetric point cloud and MBES data

4 Summary and outlook

The purpose of this feasibility study was to fuse MBES data with 3D point clouds derived from photogrammetric image triangulation in order to improve data density. The paper presents a processing chain for combining hybrid point clouds generated from photogrammetric imagery and hydroacoustic systems. MBES data hereby posed an initial starting point thanks to its good absolute positioning accuracy and thus was used to georeference and scale all further data. The point cloud from imagery was then to be transformed to best match the MBES data via ICP.

The resulting data set provides an objective representation of a wreck, suitable for improved decision-making concerning underwater obstructions. It shows good congruence of MBES data with the photogrammetric point cloud. Even though, apart from the MBES data, no independent scale could be included for this data set, it is observable that the deviations between the two data sets achieves an expected level of precision of 5.3 cm. Major deviations result mostly in areas that are hard to ensonify by the MBES (i.e. occluded areas near the seafloor) and on the edge of the photogrammetric point cloud with probably fewer measurement samples and a worse acquisition geometry. The surface density is highly improved by several orders of magnitude due to the imagery-derived point cloud.

For point cloud registration, initial values were obtained by manually selecting salient points such as the bow in the imagery. Determining correspondence between the salient points in both point clouds was quite challenging due to missing local geometric gradients on the wreck's starboard side. Automatic detection by suitable feature detectors or marked positions should significantly improve this processing step and avoid manual interaction in future works. Furthermore, colour information was included by this fusion using image enhancement as a preprocessing step. With this method, a green colour cast was removed and a more natural representation of the wreck was thus achieved. Though processing times of photogrammetric data may go up to several hours or even days with large data sets, many processing steps can be automated to a certain degree.

During the underwater image acquisition, several practical problems occurred which had to be taken into account when performing observations from a ROV and integrating a camera system. The tether connected to the ROV was often tangling around edges of the wreck, thus limiting manoeuvrability. Furthermore, the cable of the camera was a regular Ethernet cable that had not been especially ruggedised for high sea applications and was rather short (70 m). This resulted in only parts of the starboard side of the wreck being observed. Future developments will lead to improvements on these issues. Since turbid water conditions required short acquisition distances of approximately 1 m, the remote control was a challenging task as well. Currents, tides and tether entanglement often interfered with the operating commands and thus affected the movement of the ROV. Therefore, practice and careful manoeuvring during such challenging acquisitions are imperative.

The presented workflow is not restricted to a ROV-borne data acquisition. Continuous developments in sensor technology leads to miniaturised sensors that allow diver-based applications, too. In this context, the integration of additional sensors on the measurement platform providing complemental information (such as sonar and inertial measurement unit) is also part of our future work.

It can be concluded that the photogrammetric method provides a higher grade of detail and accuracy, even when observing geometrically challenging structures, such as a sidewall providing only very low geometric information in line of sight, posing a dead reckoning problem. Using image enhancement, significant contrast increase could be achieved, resulting in more images being aligned and higher coverage of the wreck. This ap-

proach is further warranted in turbid water, such as the Baltic Sea, where visibility rarely exceeds one to two metres. The resulting georeferenced high density point cloud can be further attributed with RGB information from the cameras, as well as the intensities of the backscattered MBES signals. The oriented camera stations are furthermore available in the coordinate system of the MBES data and can be used for further investigations on the wreck's condition. Spatial data infrastructures of maritime administrations benefit from these added values for improved decision-making. //

Acknowledgements

The authors thank the *Deneb* crew for their great support during the experiments. This work is partially funded by Volkswagen Foundation (ZN3253).

References

Akkaynak, Derya; Tali Treibitz (2019): Sea-Thru. A Method for Removing Water From Underwater Images. 2019 IEEE/CVF Conference on Computer Vision and Pattern Recognition (CVPR), DOI: 10.1109/CVPR.2019.00178

Besl, Paul J.; Neil D. McKay (1992): A method for registration of 3-D shapes. IEEE Transactions on Pattern Analysis and Machine Intelligence, DOI: 10.1109/34.121791

Bianco, Gianfranco; Maurizio Muzzupappa et al. (2015): A new color correction method for underwater imaging. ISPRS – International Archives of the Photogrammetry, Remote Sensing and Spatial Information Sciences XL-5/W5, DOI: 10.5194/isprsarchives-XL-5-W5-25-2015

Brissette, Michel B.; John E. Hughes-Clarke et al. (1997): Detecting small seabed targets using a high frequency multibeam sonar: geometric models and test results. Oceans '97. MTS/IEEE Conference Proceedings, DOI: 10.1109/OCEANS.1997.624099

Brown, Duane C. (1971): Close-Range Camera Calibration. Photogrammetric Engineering, No. 8, pp. 855–866

BSH (2020): Wreck search – Basics. www.bsh.de/EN/TOPICS/Surveying_and_cartography/Wreck_search/Basics/basics_node.html

Drap, Pierre; Djamel Djamal Merad et al. (2015): Underwater Photogrammetry and Object Modeling. A Case Study of Xlendi Wreck in Malta. Sensors, DOI: 10.3390/s151229802

Durrant-Whyte, Hugh; Tim Bailey (2006): Simultaneous localization and mapping. Part I. IEEE Robotics & Automation Magazine, DOI: 10.1109/MRA.2006.1638022

Engel, Jakob; Jörg Stückler; Daniel Cremers (2015): Large-scale direct SLAM with stereo cameras. 2015 IEEE/RSJ International Conference on Intelligent Robots and Systems (IROS), DOI: 10.1109/IROS.2015.7353631

Fabri, Marie-Claire; Beatriz Vinha et al. (2019): Evaluating the ecological status of cold-water coral habitats using non-invasive methods. An example from Cassidaigne canyon, northwestern Mediterranean Sea. Progress in Oceanography, DOI: 10.1016/j.pocean.2019.102172

Fischler, Martin A.; Robert C. Bolles (1981): Random sample consensus. A paradigm for model fitting with applications to image analysis and automated cartography. Communications of the ACM, DOI: 10.1145/358669.358692

Furukawa, Yasutaka; Jean Ponce (2010): Accurate, Dense, and Robust Multiview Stereopsis. IEEE Transactions on Pattern Analysis and Machine Intelligence, DOI: 10.1109/TPAMI.2009.161

Hirschmüller, Heiko (2008): Stereo Processing by Semi-Global Matching and Mutual Information. IEEE Transactions on Pattern Analysis and Machine Intelligence, DOI: 10.1109/TPAMI.2007.1166

IHO (2008): IHO Standards for Hydrographic Surveys. Special Publication S-44 – Edition 5. International Hydrographic Bureau, Monaco

Jordt-Sedlazeck, Anne; Reinhard Koch (2012): Refractive Calibration of Underwater Cameras. In: Andrew Fitzgibbon; Svetlana Lazebnik et al. (Eds.): Computer Vision – ECCV 2012. Springer, DOI: 10.1007/978-3-642-33715-4_61

Kahmen, Oliver; Robin Rofallski et al. (2019): On scale definition within calibration of multi-camera systems in multimedia photogrammetry. ISPRS – International Archives of the Photogrammetry, Remote Sensing and Spatial Information Sciences XLII-2/W10, DOI: 10.5194/isprs-archives-XLII-2-W10-93-2019

Kim, Ayoung; Ryan M. Eustice (2013): Real-Time Visual SLAM for Autonomous Underwater Hull Inspection Using Visual Saliency. IEEE Transactions on Robotics, DOI: 10.1109/TRO.2012.2235699

Kotowski, Rüdiger (1988): Phototriangulation in Multi-Media Photogrammetry. International Archives of Photogrammetry and Remote Sensing (Vol. XXVII), pp. 324–334

Low, Kok-Lim (2004): Linear Least-Squares Optimization for Point-to-Plane ICP Surface Registration. Technical Report TR04-004, University of North Carolina at Chapel Hill

Luhmann, Thomas; Stuart Robson et al. (2020): Close-Range Photogrammetry and 3D Imaging, 3rd revised and expanded edition. De Gruyter, Berlin, Boston, DOI: 10.1515/9783110607253

Maas, Hans-Gerd (1995): New developments in Multimedia Photogrammetry. In: Armin Grün; Heribert Kahmen (Eds.): Optical 3D Measurement Techniques III. Wichmann, Karlsruhe, pp. 362–372

Mangeruga, Marino; Fabio Bruno et al. (2018): Guidelines for Underwater Image Enhancement Based on Benchmarking of Different Methods. Remote Sensing, DOI: 10.3390/rs10101652

Menna, Fabio; Erica Nocerino et al. (2016): Geometric and Optic Characterization of a Hemispherical Dome Port for Underwater Photogrammetry. Sensors (Basel), DOI: 10.3390/s16010048

Mur-Artal, Raul; Juan D. Tardós (2017): ORB-SLAM2. An Open-Source SLAM System for Monocular, Stereo and RGB-D Cameras. IEEE Transactions on Robotics, DOI: 10.1109/TRO.2017.2705103

Nocerino, Erica; Fabio Menna et al. (2016): Underwater calibration of dome port pressure housings. ISPRS – International

Archives of the Photogrammetry, Remote Sensing and Spatial Information Sciences XL-3/W4, DOI: 10.5194/isprsarchives-XL-3-W4-127-2016

Nocerino, Erica; Mohamad Nawaf et al. (2018): Multi-camera system calibration of a low-cost remotely operated vehicle for underwater cave exploration. ISPRS – International Archives of the Photogrammetry, Remote Sensing and Spatial Information Sciences XLII-1, DOI: 10.5194/isprs-archives-XLII-1-329-2018

Nornes, Stein M.; Martin Ludvigsen et al. (2015): Underwater Photogrammetric Mapping of an Intact Standing Steel Wreck with ROV. IFAC-PapersOnLine, DOI: 10.1016/j.ifacol.2015.06.034

Prado, Elena; Maria Gómez-Ballesteros et al. (2019): 3D Modeling of Rio Miera Wreck Ship Merging Optical and Multibeam High Resolution Points Cloud. ISPRS - International Archives of the Photogrammetry, Remote Sensing and Spatial Information Sciences XLII-2/W10, DOI: 10.5194/isprs-archives-XLII-2-W10-159-2019

Przybilla, Heinz-Jürgen; Rüdiger Kotowski et al. (1990): Geometrical Quality Control in Nuclear Power Stations. An Application of High Precision Underwater Photogrammetry. The Photogrammetric Record, DOI: 10.1111/j.1477-9730.1990.tb00718.x

Remondino, Fabio; Maria Grazia Spera et al. (2013): Dense image matching. Comparisons and analyses. 2013 Digital Heritage International Congress (DigitalHeritage), DOI: 10.1109/DigitalHeritage.2013.6743712

Shortis, Mark (2015): Calibration Techniques for Accurate Measurements by Underwater Camera Systems. Sensors (Basel), DOI: 10.3390/s151229831

Snavely, Noah; Steven M. Seitz; Richard Szeliski (2006): Photo tourism. Exploring photo collections in 3D. ACM Transactions on Graphics, DOI: 10.1145/1141911.1141964

Wang, Yan; Wei Song et al. (2019): An Experimental-Based Review of Image Enhancement and Image Restoration Methods for Underwater Imaging. IEEE Access, DOI: 10.1109/ACCESS.2019.2932130